NANO LETTERS

LETTER

pubs.acs.org/NanoLett

Optimized Spatial Correlations for Broadband Light Trapping Nanopatterns in High Efficiency Ultrathin Film a-Si:H Solar Cells

Vivian E. Ferry,[†,‡] Marc A. Verschuuren,[§] M. Claire van Lare,[†] Ruud E. I. Schropp,[∥] Harry A. Atwater,[‡] and Albert Polman[*,†]

[†]Center for Nanophotonics, FOM Institute AMOLF, Science Park 104, 1098 XG Amsterdam, The Netherlands

[‡]Thomas J. Watson Laboratories of Applied Physics, California Institute of Technology, Pasadena, California 91125, United States

[§]Philips Research Laboratories, High Tech Campus 4, 5656 AE Eindhoven, The Netherlands

[∥]Debye Institute for Nanomaterials Science, Section Nanophotonics, Utrecht University, P.O. Box 80.000, 3508 TA Utrecht, The Netherlands

Supporting Information

ABSTRACT: Nanophotonic structures have attracted attention for light trapping in solar cells with the potential to manage and direct light absorption on the nanoscale. While both randomly textured and nanophotonic structures have been investigated, the relationship between photocurrent and the spatial correlations of random or designed surfaces has been unclear. Here we systematically design pseudorandom arrays of nanostructures based on their power spectral density, and correlate the spatial frequencies with measured and simulated photocurrent. The integrated cell design consists of a patterned plasmonic back reflector and a nanostructured semiconductor top interface, which gives broadband and isotropic photocurrent enhancement.

KEYWORDS: Thin film solar cells, surface plasmon polariton, light trapping, nanoimprint lithography, photovoltaics, silicon

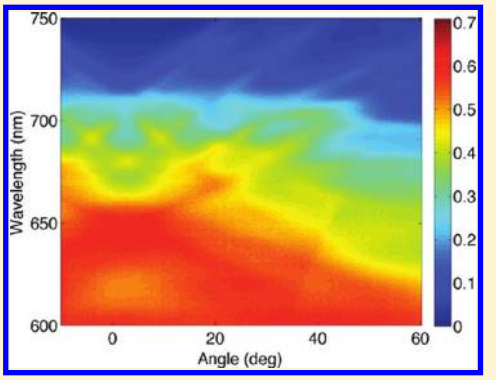

Thin and ultrathin film solar cells are attractive candidates for low-cost replacement of thick, wafer-based devices. To achieve full absorption of the solar spectrum with ultrathin semiconductor volumes, light trapping is required over a broad spectral and angular range. To date, several light trapping geometries based on nanowires, nanocones, photonic crystals, nanoparticles, gratings, and random textures have been demonstrated.[1−18] While many researchers have demonstrated increased photocurrent due to scattering-mediated light trapping, the role of spatial correlations and surface topography of random or periodic arrangements of the scattering nanostructures has remained unclear. Here we identify the relation between these key parameters and the photocurrent spectrum for high efficiency, ultrathin (<100 nm thick absorber) film a-Si:H solar cells containing both integrated plasmonic and Mie scattering nanostructures. The nanostructure arrays described here are defined by their spatial coherence spectral density and are designed for broadband and isotropic response in ultrathin semiconductor volumes.

Ultrathin film solar cells possess a number of advantages over their thicker counterparts. Ultrathin films are less expensive due to the reduced cost of raw materials. For technologies based on scarce elements, such as CdTe and $CuIn_xGa_{1-x}Se_2$, a thickness reduction could expand scalability to the terawatt range.[7,19] For thin film Si cells, the use of ultrathin layers translates into faster manufacturing throughput, as overall cell production times are often limited by the chemical vapor deposition rate of the semiconductor film. For hydrogenated amorphous Si (a-Si:H) the use of ultrathin layers in addition strongly reduces the photodegradation that is commonly observed in thick cells due to the increased electric field across the ultrathin p-i-n junction.[20,21] Moreover, for semiconductors that are not surface recombination limited, a reduction in semiconductor thickness leads to higher open-circuit voltages due to decreased bulk recombination.[22] While all of the above factors indicate that reducing semiconductor layer thickness is advantageous for the fabrication of inexpensive, stable, thin-film solar cells with high open circuit voltage, the major opposing requirement that limits the thickness is light absorption: to harvest the full solar spectrum the cell needs to be "optically thick" for wavelengths up to the semiconductor bandgap.

Light-trapping nanostructures allow for nanoscale control of the direction and absorption of light in ultrathin film solar cells, enabling new designs in which light is absorbed in semiconductor volumes much thinner than the optical absorption length. Indeed, an ultrathin film solar cell can be considered as an optical integrated circuit in which light is received, guided, localized, and collected at the nanoscale. Inspired by optoelectronics, plasmonic nanostructures have recently attracted attention for light trapping in solar cells due to their large resonant scattering cross sections. Here we use plasmonic metal nanostructures integrated

Received: July 1, 2011
Revised: August 23, 2011
Published: August 29, 2011

into the back contact of the solar cell to couple light into in-plane waveguide modes of the thin semiconductor layer, thereby increasing the path length and the short circuit current density (J_{sc}).[7,18,19] The additional layers of the solar cell conformally coat the Ag back contact, producing a three-dimensional solar cell with a nanostructured top interface composed of Mie scatterers, leading to light trapping into localized modes near the surface as well.

Most light-trapping geometries studied, particularly for a-Si:H, are based on random scattering structures with the geometry determined by the random nature of a deposition, growth, or etch process rather than by design. This is due to the fact that no suitable techniques were available that enable the controlled fabrication of engineered random scattering arrays at low cost. Recently, soft imprint lithography has been introduced as a technique that enables large-area, inexpensive fabrication of arrays of nanoscatterers.[23−26] We have shown that periodic arrays made using this technique show enhanced photocurrents in ultrathin film a-Si:H solar cells over a narrow spectral range.[8] This new technique now also enables the design and fabrication of engineered random arrays with the spatial frequencies in the array pattern optimized for trapping a broad solar spectral band that is otherwise poorly absorbed. In this paper, we systematically design and fabricate periodic and random arrays of nanoscatterers integrated in the back contact of an a-Si:H solar cell. By tailoring the spatial frequencies and obtaining an integrated understanding of both the localized and propagating modes resulting from plasmonic and Mie scattering in the three-dimensional structure, we are able to demonstrate an extremely thin cell with broadband photocurrent enhancement in both the blue and the red portions of the spectrum.

The fabrication process utilizes Substrate Conformal Imprint Lithography (SCIL), a wafer-scale nanoimprint lithography process to inexpensively replicate high fidelity, large area nanopatterns into silica sol−gel resist, which has been described in detail elsewhere.[8,23−26] An initial large-area master substrate was patterned using electron-beam lithography on a Si wafer. The master substrate consists of 84 patterned regions containing one of 12 nanopatterns, tiled with repetition and rotation to control for deposition inhomogeneities, where each pattern covers a 6 mm × 6 mm area and the total master area is 10 cm × 3.6 cm. A bilayer stamp was molded from the master, consisting of a thin high-modulus polydimethylsiloxane (PDMS) layer holding the nanopatterns and a low-modulus PDMS layer to bond the rubber to a 200 μm thick glass support for in-plane stiffness. The stamp was used to emboss a 100 nm thick layer of silica sol−gel on AF45 glass substrates using SCIL. The sol−gel layer solidifies at room temperature by forming a silica network, while reaction products diffuse into the rubber stamp. After stamp release the sol−gel was post cured at 200 °C.

A thirteenth nanopattern is a reference pattern replicated from Asahi U-type texture. The texture is formed via a second stamp molded from an Asahi U-type reference substrate, and the texture transferred into sol−gel resist for use as a reference.[25,26] Atomic force microscopy (AFM) comparison of the original and replica Asahi textures are in good agreement. We use a stamp transferred random texture rather than the original Asahi U-type glass substrate as both the reference and the designed nanopatterns are later coated in Ag to form the back contact, and it is more appropriate to coat identical materials. Although there are examples of other highly performing, randomly deposited growth substrates available in the literature, we use Asahi U-type

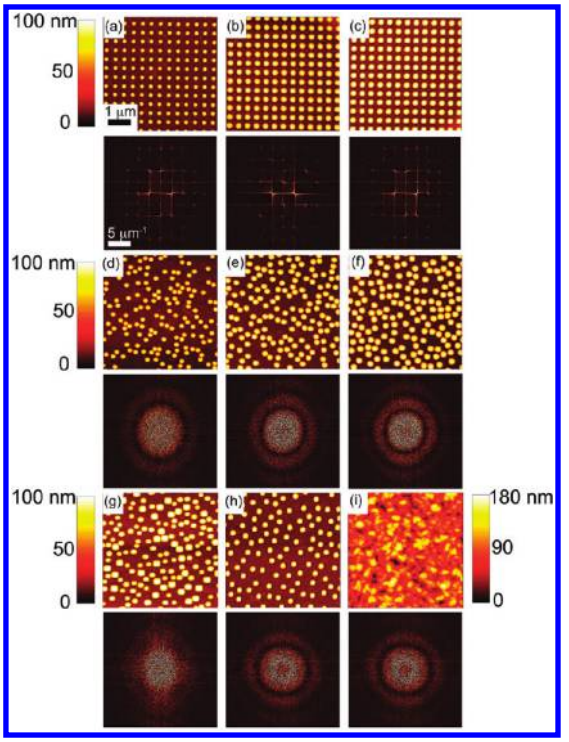

Figure 1. Metal nanopatterns used as light trapping surfaces. Four general classes of nanopatterns were fabricated on the substrate: (a−c) periodic arrays of nanoparticles with different diameters, (b−g) pseudorandom lattices of nanoparticles with controlled shape and packing density, (h) penrose lattice of nanoparticles, and (i) nanoimprint replicated Asahi U-type glass. AFM images are taken of the Ag-coated silica sol−gel imprints; the corresponding Fourier transforms are shown below.

texture as a reference not because it is the optimal texture but because it is a commercially available and state of the art laboratory standard.[14]

The 13 nanopatterns chosen fall into a few categories: flat, periodic (square lattices of 400 and 500 nm pitch), pseudorandom (with controlled nanoparticle size), quasicrystal (penrose pattern), and randomly textured (Asahi replica). Both the Asahi reference and the designed nanopattern imprinted silica sol−gel surfaces are overcoated with Ag via sputtering to form the metallic back contact. The designed individual nanostructures consist of rounded plasmonic hemiellipsoidal nanostructures after Ag coating. Figure 1 shows AFM images of representatives of the Ag-coated patterns, along with their two-dimensional Fourier transforms. The nanoparticle sizes and shape are seen to be uniform across the substrate. Three sizes of nanoparticles were used in separate patterns, denoted small, medium, and large, corresponding to 200, 290, and 310 nm diameter, respectively. For the pseudorandom patterns, each pattern was uniquely generated with the constraints that the Ag particles do not touch after overcoating, and that the packing fraction is the same as for the 400 nm periodic pattern. The three different pseudorandom patterns differ in the diameter of the nanoparticles, which in turn sets a minimum separation between particles due to the non-overlapping constraint. A more detailed discussion of the pattern-generation procedure is included in the Supporting Information. As discussed later, the rounded metal nanostructures are advantageous, as they avoid the high parasitic absorption associated

dx.doi.org/10.1021/nl202226r |*Nano Lett.* 2011, 11, 4239–4245

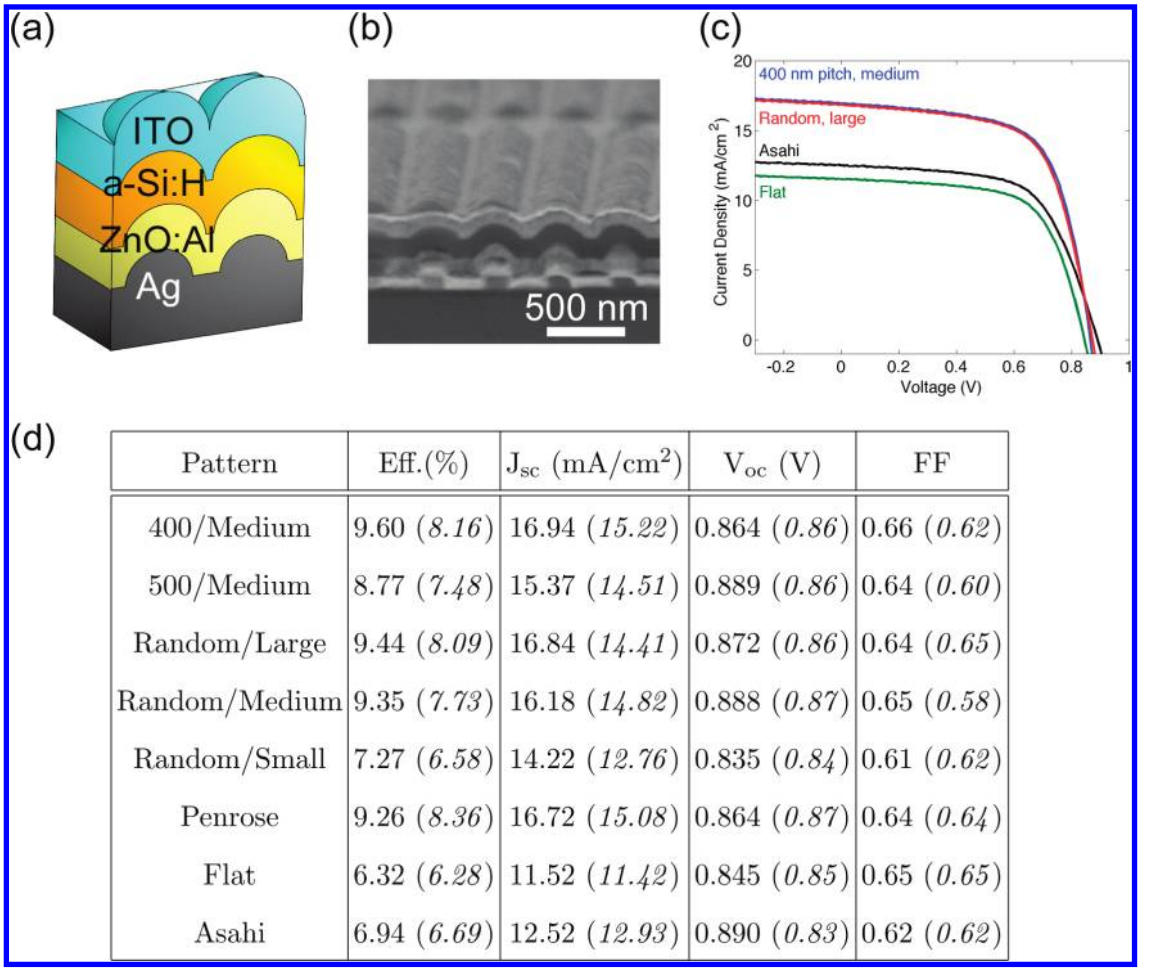

(d)

Pattern	Eff.(%)	J_{sc} (mA/cm^2)	V_{oc} (V)	FF
400/Medium	9.60 (*8.16*)	16.94 (*15.22*)	0.864 (*0.86*)	0.66 (*0.62*)
500/Medium	8.77 (*7.48*)	15.37 (*14.51*)	0.889 (*0.86*)	0.64 (*0.60*)
Random/Large	9.44 (*8.09*)	16.84 (*14.41*)	0.872 (*0.86*)	0.64 (*0.65*)
Random/Medium	9.35 (*7.73*)	16.18 (*14.82*)	0.888 (*0.87*)	0.65 (*0.58*)
Random/Small	7.27 (*6.58*)	14.22 (*12.76*)	0.835 (*0.84*)	0.61 (*0.62*)
Penrose	9.26 (*8.36*)	16.72 (*15.08*)	0.864 (*0.87*)	0.64 (*0.64*)
Flat	6.32 (*6.28*)	11.52 (*11.42*)	0.845 (*0.85*)	0.65 (*0.65*)
Asahi	6.94 (*6.69*)	12.52 (*12.93*)	0.890 (*0.83*)	0.62 (*0.62*)

Figure 2. Current−voltage characteristics of nanopatterned cells. The cells are conformally deposited over the patterned substrate, as shown schematically in (a) and in SEM cross section (5° angle) in (b). The maximum particle diameter in the backpattern was chosen so that nanostructures in the ITO top layer would touch without overlap. (c) Current density−voltage measurements for the best-efficiency cells on the substrate with 90 nm intrinsic layers. The optimized periodic pattern and the pseudorandom pattern have efficiencies of 9.6 and 9.4%, respectively. (d) Electrical characteristics of highest-efficiency cells with average values shown in parentheses.

with sharp metallic features and they allow for conformal growth of the a-Si:H to produce both front and back textures. The diameters and pitch of the periodic nanopatterns were chosen based on electromagnetic simulations that account for the conformal deposition of all the cell layers over the patterns. The top indium tin oxide (ITO) surface of the cell shows a pattern of nanodomes as a result of the conformal depositions over the Ag back contact, and the best performance is predicted for Ag diameters and pitches such that the ITO nanostructures are at maximum packing density without overlap, as illustrated schematically in Figure 2a.

Cells were deposited over identical substrates with three different intrinsic layer thicknesses: 90, 115, and 150 nm. The cells consist of 100 nm of Ag coating the patterned silica sol−gel, 130 nm of ZnO:Al deposited by sputtering, n-i-p a-Si:H of varying i-layer thickness, 80 nm of ITO, and evaporated Au finger contacts. Device cross sections were made by a CO_2 laser along the backside of the cells, which lead to controlled splitting of the samples leading to clean cross sections. The cut samples were then imaged with scanning electron microscopy. Figure 2b shows a cross section through the cell illustrating the conformal nature of the growth. The top surface structure was also verified using AFM.

Figure 2c shows current−voltage measurements on the cells with 90 nm intrinsic layers for some selected cell patterns. Device characterization was performed using a dual source WACOM solar simulator under one sun illumination (AM1.5, 100 mW/cm^2). A table summarizing the results for each pattern for this thickness is shown in Figure 2d with the additional thicknesses and patterns described in Supporting Information Tables 1−3. Over 1000 cells were measured in total for this study, and the tabulated data reports the highest efficiency measured for each pattern at each deposition run, with the average value of three cells on the substrate shown in parentheses. We estimate the error in the solar simulator to be ±3%, the variation in J_{sc} at 7%, the V_{oc} 3%, and the fill factor 5%.

Several important trends are observed from comparison of the nanopatterns. The cells of 400 nm pitch have higher J_{sc} than those with 500 nm pitch. Cells with large and medium diameter nanoparticles show higher currents than those with small nanoparticles. The highest efficiency (9.4−9.6%) for the thinnest ultrathin layers is observed for the 400 nm pitch pattern with medium particles and the random pattern with large particles. These two patterns consistently perform well at other intrinsic layer thicknesses. These efficiencies are among the highest measured

dx.doi.org/10.1021/nl202226r |*Nano Lett.* 2011, 11, 4239–4245

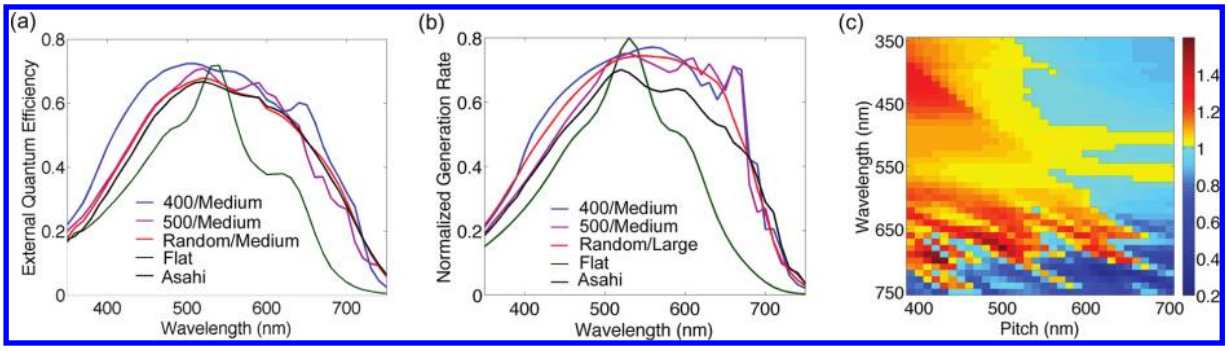

Figure 3. External quantum efficiency measurements and simulations. (a) External quantum efficiency measurements for several different patterns with 90 nm intrinsic layer thickness. (b) Simulated absorption for the same nanopatterns as in (a). (c) Electromagnetic simulations of absorption enhancement as a function of pitch for cells with 115 nm intrinsic layer thickness. The color scale indicates the absorption enhancement compared to a simulated Asahi cell of the same thickness.

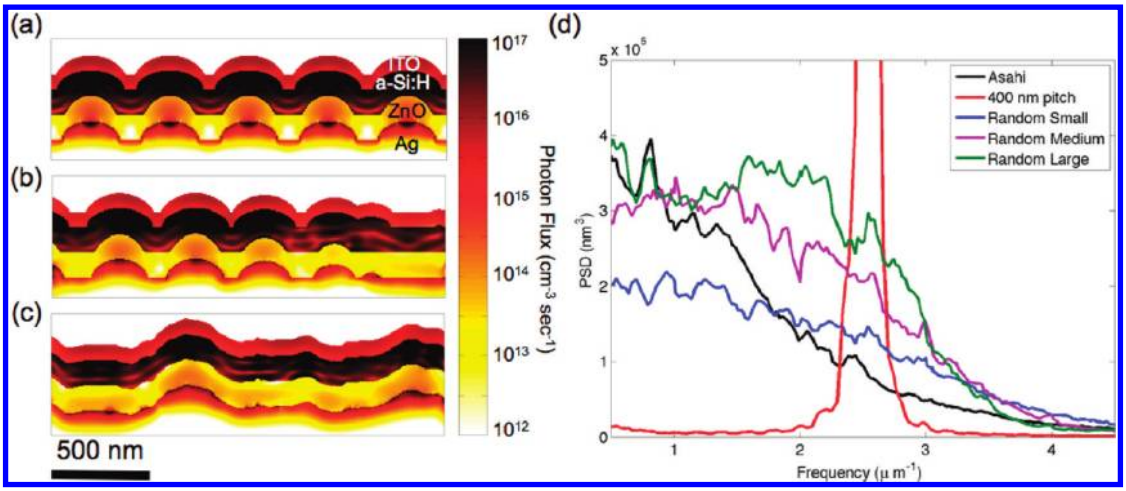

Figure 4. Pseudorandom and randomly textured patterns. (a) Photon flux in all layers of the solar cell calculated from electromagnetic simulation for cells with a 400 nm pitch periodic array, (b) simulation for pseudorandom particle array, (c) simulation for Asahi U-type texture. (d) One-dimensional power spectral density calculations based on AFM data from Figure 1. The 400 nm pitch and pseudorandom patterns with large particles have the highest power through the range of spatial frequencies required for coupling to waveguide modes in the a-Si/H in the 600−700 nm spectral band.

for nanostructured a-Si:H solar cells and are especially notable given the very small (90 nm) intrinsic layer thickness.

External quantum efficiency (EQE) measurements for representative cells with a 90 nm intrinsic a-Si/H layer are shown in Figure 3a, and results for full-field three-dimensional electromagnetic simulations for similar structures in Figure 3b. EQE measurements were performed using monochromatic light from a Xenon lamp with one sun light bias applied. All of the textured and nanopatterned devices show enhanced photocurrent on the red side of the spectrum. Notably the photocurrent of the 400 nm pitch cell is also enhanced on the blue side of the spectrum.[4,10,11,27] On the red side of the band, there are several sharp peaks in the periodic nanopatterns that are correlated with pitch. We have previously shown these features are due to waveguide modes with high overlap with the a-Si:H.[8] In these cells, the ZnO:Al layer acts not only as a diffusion buffer layer between a-Si:H and Ag but also optically separates the a-Si:H waveguide modes from the lossy surface plasmon polariton modes on the metallic interface.[8,28]

We also note that the value of J_{sc} obtained from integrating the EQE spectra against the AM1.5 solar spectrum is lower than the values reported in Figure 2d. This is a well-known issue in measuring solar cells and may be due to many different effects. In general, spectral mismatch between the EQE source and the solar simulator can cause a discrepancy between the two measurements, underestimating the current from the EQE spectra. Also, the EQE spectra shown are representative of the different patterns rather than the best devices and were measured before additional annealing steps that improved the cell performance. Furthermore, these cells are sensitive to the angle of incidence of illumination, and perform better at off-normal incidence (discussed later in the text). The EQE measurements use a tightly focused source, while the solar simulator has a slight angular distribution, which will give different values for the current.

The experimental trends correspond well with those predicted from simulation, including the strong enhancement in the blue portion of the spectrum. The simulation details are given in the Supporting Information. Given that the electromagnetic simulation technique accounts only for optical absorption and not carrier collection, the observed increase on the blue side is likely due to light trapping and not differences in the p-layer thickness or deposition. Figure 3c shows the calculated absorption enhancement as a function of pitch from 400−700 nm for periodic arrays with d_{Ag}= 300 nm and d_{ITO}= 400 nm (thus limiting the

dx.doi.org/10.1021/nl202226r |*Nano Lett.* 2011, 11, 4239–4245

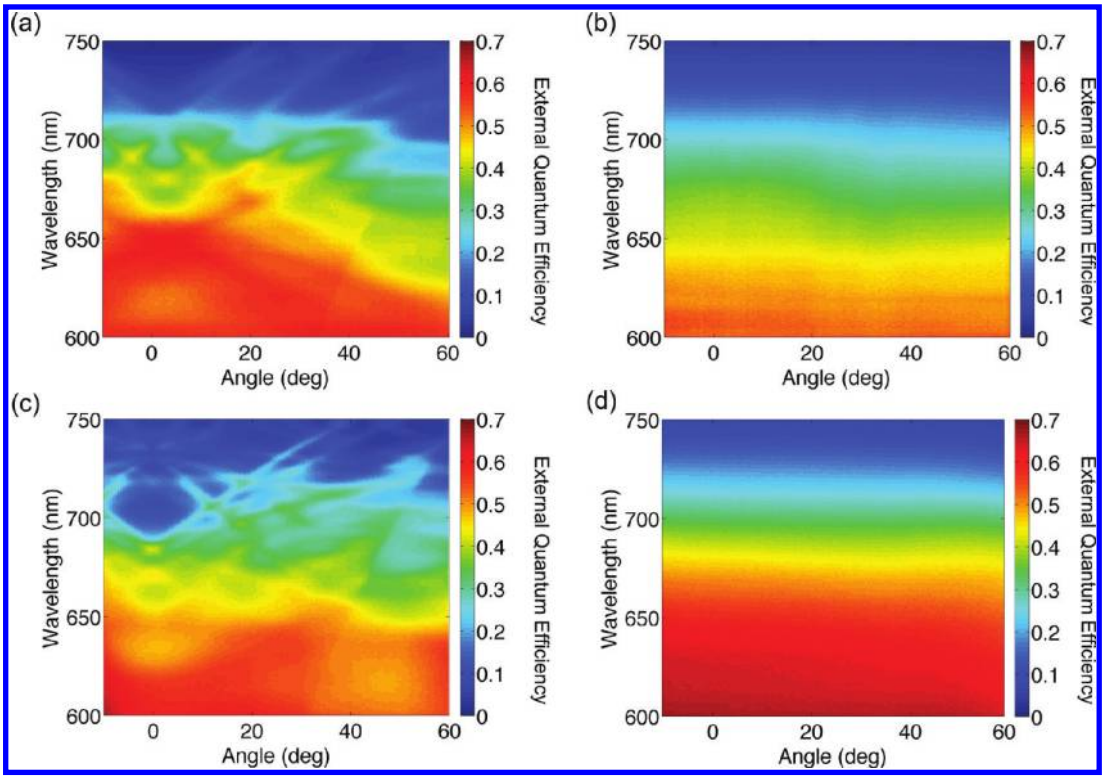

Figure 5. Experimental measurements of angle-resolved photocurrent on red side of spectrum. (a) A 400 nm pitch pattern on 90 nm cell. (b) Pseudorandom pattern with varying particle sizes on 90 nm thick cell. (c) A 400 nm pitch pattern on cell with 150 nm thickness. (d) Pseudorandom pattern with large particles on 150 nm thick cell. The periodically patterned cells show signatures of coupling to waveguide modes, while the pseudorandom nanopatterns show isotropic angular response.

pitch to 400 nm to avoid overlapping nanodomes). The color scale shows the absorption enhancement relative to a simulated Asahi cell. On the red side of the spectrum, we observe branches due to coupling to waveguide modes as discussed previously with the resonant peaks shifting with pitch. On the blue side of the spectrum, there is a broad range of absorption enhancement that cuts off sharply at wavelengths shorter than the pitch.

At wavelengths where the absorption length in a-Si:H is shorter than the scatterer separation, the absorption is mostly due to localized modes. Figure 4a−c shows photon flux cross sections from simulation for the periodic and pseudorandom patterns at λ = 500 nm. The absorption is largely confined over each scatterer, as can be seen by the similarities in the absorption over the a-Si/H. Of course only the absorption in the a-Si/H contributes to photocurrent, but the images in Figure 4a−c also show the losses in the other layers, indicating that the ITO is a significant source of parasitic absorption. Figure 4a−c also illustrates the importance of nanostructure curvature. Plasmonic nanostructures with high frequency shapes (i.e., sharp points) are highly absorbing, leading to parasitic absorption in the metal layer (Figure 4c). In contrast, both the periodic and pseudorandom designed nanoarrays control the nanoparticle shape to include only rounded, curved scatterers (Figure 4a,b).

When the absorption length in a-Si:H is longer than the separation between particles (for λ > 600 nm) the arrangement of the nanoparticles becomes more important and the incident sunlight will couple to propagating modes of the device. In the periodic case coupling only occurs for wavelengths where the pattern bridges the wavevector mismatch between incoming light and waveguide modes, leading to the photocurrent peaks in the EQE spectrum of Figure 3a. Similarly, the designed pseudorandom nanopatterns result in efficient coupling to waveguide modes, but now over a broader spectral range, leading to a smooth EQE spectrum.

To quantitatively understand the connection between the nanopatterns and the observed strong photocurrent enhancement, in particular for the pseudorandom patterns, we calculated the power spectral density (PSD)[29] of the patterned back contacts from the AFM data shown in Figure 1. The results are shown in Figure 4d. The periodic, 400 nm pitch pattern, unsurprisingly, has a very sharp band centered at 2.5 μm^{-1} with a bandwidth due to the finite size of the AFM scan. The Asahi and pseudorandom nanopatterns are much broader and flatter in spatial frequency.

To realize coupling to waveguide modes over the broadest possible solar spectral range requires a pattern with flat PSD through the range of spatial frequencies required to couple to the waveguide modes of the a-Si:H and at the same time minimal scattering power in the nondesirable spectral ranges. Within this framework, we can now explain the observed trends in photocurrent and deduce essential design rules. First, we observe that the pseudorandom patterns have higher scattering power than the Asahi texture through the range of optical frequencies required (Figure 4d). Indeed, the cells with engineered random patterns show much better cell performance than the Asahi cells (Figures 2, 3). Second, the large nanoparticles have higher scattering power than the smaller nanoparticles, consistent with the better light trapping observed for larger particles in both the periodic and pseudorandom arrays. Third, the periodic array is too narrowband to act as an isotropic light trapping surface.

dx.doi.org/10.1021/nl202226r |*Nano Lett.* 2011, 11, 4239–4245

While the PSD argument explains many of the observations of light trapping on the red side of the spectrum, it does not explain the strong photocurrent enhancement on the blue side of the spectrum. Since the absorption length of a-Si/H is under 100 nm in the λ= 400−500 nm range, the enhanced photocurrent on the blue side must be due to the nanostructuring on the top interface. From simulation, we attribute this to the ITO/a-Si:H hemispherical nanostructures acting as weakly coupled Mie resonators, such that incident sunlight is resonantly absorbed in the hemisphere[30] and forward scattered into the a-Si:H region. The effective interaction cross section of these scatterers is 3−4 times their geometrical area over a broad UV/blue spectral range and thus leads to enhanced incoupling of light at these wavelengths, for which light would otherwise be strongly reflected. This enhancement in the UV/blue is consistent with the simulation results shows in Figure 3c and the 400 nm pitch was chosen a priori from these simulations at it showed the highest solar spectrum integrated absorption.

Finally, we measured the angle-resolved EQE for the nanopatterned cells. Data are shown for 400 nm pitch and pseudorandom cells with a 90 nm (Figure 5a,b) and 150 nm (Figure 5c,d) intrinsic a-Si:H layer. The periodic cells show signatures of waveguide modes in the semiconductor, which shift with changing angle of incidence. We observe a higher number of mode branches in Figure 5c than in Figure 5a, due to the higher mode density in the thicker a-Si:H layer. In contrast, the engineered random nanopatterns show an isotropic response with angle (Figure 5b,d). To achieve isotropic light trapping, a range of spatial frequencies must be present in the pattern to efficiently couple all angles into the localized and waveguide modes of the cell.

In summary, systematic study and design of pseudorandom arrays of resonantly scattering nanoparticles allow for both an understanding of the ideal random patterns for broadband, isotropic angular response, and the realization of high efficiency devices in extraordinarily thin semiconductor regions. Key to the design is an integrated understanding of spatial frequencies and curvature of nanoscale scatterers that form plasmonic backreflectors coupling to waveguide modes and weakly coupled surface Mie scatterers coupling to localized surface modes. While the diameters and pitch of the front and back surface patterns in this study were designed with a one-step, conformal deposition process in mind, it is possible that decoupling the pattern formation at the two interfaces will lead to higher overall efficiencies, extending the applicability to nonconformal semiconductor depositions. While focused here on a-Si:H, the principles presented here are potentially applicable to other solar cell materials systems.

■ ASSOCIATED CONTENT

Supporting Information. Additional information and figures. This material is available free of charge via the Internet at http://pubs.acs.org.

■ AUTHOR INFORMATION

Corresponding Author
*E-mail: polman@amolf.nl.

■ ACKNOWLEDGMENT

We are grateful to Karine van der Werf for solar cell depositions, to MiPlaza for electron-beam fabrication of the master pattern, and to Michael Kelzenberg, Krista Langeland, Imogen Pryce, Piero Spinelli, Robert Walters, Jorik van der Groep, and David Valley for useful discussions and assistance with the manuscript. The Caltech portion of this work was supported by the Department of Energy under contract number DE-FG02-07ER46405 (modeling) and SETP GO-18006 (cell fabrication). Work at AMOLF is part of the research program of FOM that is financially supported by NWO. This work is also part of the Global Climate and Energy Project (GCEP).

■ REFERENCES

(1) Kelzenberg, M. D.; Boettcher, S. W.; Petykiewicz, J. A.; Turner-Evans, D. B.; Putnam, M. C.; Warren, E. L.; Spurgeon, J. M.; Briggs, R. M.; Lewis, N. S.; Atwater, H. A. Enhanced absorption and carrier collection in Si wire arrays for photovoltaic applications. *Nat. Mater.* **2010**, *9*, 239–244.

(2) Law, M.; Greene, L. E.; Johnson, J. C.; Saykally, R.; Yang, P. D. Nanowire dye-sensitized solar cells. *Nat. Mater.* **2005**, *4*, 455–459.

(3) Zhu, J.; Hsu, C.-M.; Yu, Z.; Fan, S.; Cui, Y. Nanodome solar cells with efficient light management and self-cleaning. *Nano Lett.* **2010**, *10*, 1989–1984.

(4) Naughton, M. J.; Kempa, K.; Ren, Z. F.; Gao, Y.; Rybczynski, J.; Argenti, N.; Gao, W.; Wang, Y.; Peng, Y.; Naughton, J. R.; McMahon, G.; Paudel, T.; Lan, Y. C.; Burns, M. J.; Shepard, A.; Clary, M.; Ballif, C.; Haug, F.-J.; Söderström, T.; Cubero, O.; Eminian, C. Efficient nanocoax-based solar cells. *Phys. Status Solidi RRL* **2010**, *4*, 181–183.

(5) Biswas, R.; Bhattacharya, J.; Lewis, B.; Chakravarty, N.; Dalal, V. Enhanced nanocrystalline silicon solar cell with a photonic crystal back-reflector. *Sol. Energy Mat. Sol. Cells* **2010**, *94*, 2337–2342.

(6) Mallick, S. B.; Agrawal, M.; Peumans, P. Optimal light trapping in ultra-thin photonic crystal crystalline silicon solar cells. *Opt. Express* **2010**, *18*, 5691–5706.

(7) Atwater, H. A.; Polman, A. Plasmonics for improved photovoltaic devices. *Nat. Mater.* **2010**, *9*, 205–213.

(8) Ferry, V. E.; Verschuuren, M. A.; Li, H. B. T.; Verhagen, E.; Walters, R. J.; Schropp, R. E. I.; Atwater, H. A.; Polman, A. Light trapping in ultrathin plasmonic solar cells. *Opt. Express* **2010**, *18*, A237–A245.

(9) Isabella, O.; Campa, A.; Heijna, M. C. R.; Soppa, W.; van Ervan, R.; Franken, R. H.; Borg, H.; Zeman, M. Diffraction gratings for light trapping in thin-film silicon solar cells. 23rd European Photovoltaic Solar Energy Conference, 1−5 September 2008, Valencia, Spain, 2025.

(10) Eisele, C.; Nebel, C. E.; Stutzmann, M. Periodic light coupler gratings in amorphous thin film solar cells. *J. Appl. Phys.* **2001**, *89*, 7722.

(11) Haase, C.; Stiebig, H. Thin-film silicon solar cells with efficient periodic light trapping texture. *Appl. Phys. Lett.* **2007**, *91*, 061116.

(12) Shir, D.; Yoon, J.; Chanda, D.; Ryu, J. H.; Rogers, J. A. Performance of ultrathin silicon solar microcells with nanostructures of relief formed by soft imprint lithography for broad band absorption enhancement. *Nano Lett.* **2010**, *10*, 3041–3046.

(13) Franken, R. H.; Stolk, R. L.; Li, H.; van der Werf, C. H. M.; Rath, J. K.; Schropp, R. E. I. Understanding light trapping by light scattering textured back electrodes in thin film n-i-p-type silicon solar cells. *J. Appl. Phys.* **2007**, *102*, 014503.

(14) Rockstuhl, C.; Fahr, S.; Bittkau, K.; Beckers, T.; Carius, R.; Haug, F.-J.; Söderström, T.; Ballif, C.; Lederer, F. Comparison and optimization of randomly textured surfaces in thin-film solar cells. *Opt. Express* **2010**, *18*, A335–A342.

(15) Yue, G.; Sivec, L.; Owens, J. M.; Yan, B.; Yang, J.; Guha, S. Optimization of back reflector for high efficiency hydrogenated nanocrystalline silicon solar cells. *Appl. Phys. Lett.* **2009**, *95*, 263501.

(16) Müller, J.; Rech, B.; Springer, J.; Vanecek, M. TCO and light trapping in silicon thin film solar cells. *Sol. Energy* **2004**, *77*, 917–930.

(17) Sai, H.; Jia, H.; Kondo, M. Impact of front and rear texture of thin-film microcrystalline silicon solar cells on their light trapping properties. *J. Appl. Phys.* **2010**, *108*, 045505.

(18) Ferry, V. E.; Sweatlock, L. A.; Pacifici, D.; Atwater, H. A. Plasmonic nanostructure design for efficient light coupling into solar cells. *Nano Lett.* **2008**, *8*, 4391–4397.

(19) Ferry, V. E.; Munday, J. N.; Atwater, H. A. Design considerations for plasmonic photovoltaics. *Adv. Mater.* **2010**, *22*, 4795–4808.
(20) Staebler, D. L.; Wronski, C. R. Reversible conductivity changes in discharge-produced amorphous silicon. *Appl. Phys. Lett.* **1977**, *31*, 292.
(21) Shah, A. V.; Schade, H.; Vanecek, M.; Meier, J.; Vallat-Sauvain, E.; Wyrsch, N.; Kroll, U.; Droz, C.; Bailat, J. Thin-film Silicon Solar Cell Technology. *Prog. Photovoltaics* **2004**, *12*, 113.
(22) Campbell, P.; Green, M. A. The limiting efficiency of silicon solar-cells under concentrated sunlight. *IEEE Trans. Electron Devices* **1986**, *33*, 234–239.
(23) Verschuuren, M.; van Sprang, H. 3D photonic structures by sol-gel imprint lithography. *Mater. Res. Soc. Symp. Proc.* **2007**, *1002*, N03.
(24) Stuart, C.; Chen, Y. Roll in and roll out: a path to high-throughput nanoimprint lithography. *ACS Nano* **2009**, *3*, 2062.
(25) Söderström, K.; Escarré, J.; Cubero, O.; Haug, F.-J.; Ballif, C. UV-nano-imprint lithography technique for the replication of back reflectors for n-i-p thin film silicon solar cells. *Prog. Photovoltaics* **2011**, *19*, 202–210.
(26) Battaglia, C.; Söderström, K.; Escarré, J.; Haug, F.-J.; Domine, D.; Cuony, P.; Boccard, M.; Bugnon, G.; Denizot, C.; Despeisse, M.; Feltrin, A.; Ballif, C. Efficient light management scheme for thin film silicon solar cells via transparent random nanostructures fabricated by nanoimprinting. *Appl. Phys. Lett.* **2010**, *96*, 213504.
(27) Huang, Y.-F.; Chattopadhyay, S.; Jen, Y.-J.; Peng, C.-Y.; Liu, T.-A.; Hsu, Y.-K.; Pan, C.-L.; Lo, H.-C.; Hsu, C.-H.; Chang, Y.-H.; Lee, C.-S.; Chen, K.-H.; Chen, L.-C. Improved broadband and quasi-omnidirectional anti-reflection properties with biomimetic silicon nanostructures. *Nat. Nanotechnol.* **2007**, *2*, 770.
(28) Haug, F.-J.; Söderström, T.; Cubero, O.; Terrazoni-Daudrix, V.; Ballif, C. Influence of the ZnO layer structure on the guided mode structure in Si/ZnO/Ag multilayers. *J. Appl. Phys.* **2009**, *106*, 044502.
(29) Biscarini, F.; Samorí, P.; Greco, O.; Zamboni, R. Scaling behavior of anisotropic organic thin films grown in high vacuum. *Phys. Rev. Lett.* **1997**, *78*, 2389–2392.
(30) Cao, L.; White, J. S.; Park, J.-S.; Schuller, J. A.; Clemense, B. M.; Brongersma, M. L. Engineering light absorption in semiconductor nanowire devices. *Nat. Mater.* **2009**, *8*, 643–647.